Submitted to
Topology Proceedings

RATIONAL MAPS: JULIA SETS FROM ACCESSIBLE MANDELBROT SETS ARE NOT HOMEOMORPHIC

ELIZABETH L. FITZGIBBON AND STEFANO SILVESTRI

Abstract. In this paper we investigate the Julia sets of singularly perturbed complex rational maps of the form

$$F_\lambda(z) = z^n + \frac{\lambda}{z^d}.$$

We'll show that, for the case $n = d = 2$, two maps drawn from main cardioids of distinct accessible Mandelbrot sets containing a cycle of period m do not have homeomorphic Julia sets, unless these cardioids are complex conjugates of one another.

1. Introduction

There has been much work in recent years to understand the dynamics of the family of rational maps on the Riemann sphere, $\overline{\mathbb{C}}$, of the form

$$F_\lambda(z) = z^n + \frac{\lambda}{z^d} \tag{1.1}$$

with $n \geq 2$, $d \geq 1$, and λ a complex parameter. The Julia set of such a map is often known to be a Sierpiński curve [2]. Cases for which this is true include: when the critical orbit enters the immediate basin of infinity after two or more iterations, the parameter lies in the main cardioid of a buried baby Mandelbrot set, or the parameter lies on a buried point in a Cantor necklace. When a critical point lies in the immediate basin of attraction of a fixed point, the map has a Checkerboard Julia set [1]. In the case of a Misiurewicz-Sierpiński map, where the critical points are

2010 *Mathematics Subject Classification.* Primary 37F10.

Key words and phrases. complex polynomials, dynamical rays, Julia set, Mandelbrot set.

strictly pre-periodic to a repelling cycle, the Julia set is known to be a generalized Sierpiński gasket [6].

In this paper, we will consider the case where a critical point lies in the immediate basin of attraction of a periodic point. First, we explore the structure of the Julia sets associated to such maps. Then, for fixed n and d, we ask whether two maps, F_λ and F_μ, each with a critical point lying in the immediate basin of attraction of a point with period m will have conjugate dynamics on their Julia sets.

2. Preliminaries

For simplicity, we consider here only the cases with $n = d$, thus

$$F_\lambda(z) = z^n + \frac{\lambda}{z^n}. \tag{2.1}$$

When $\lambda = 0$ the map is just the degree-n map, $F_\lambda(z) = z^n$, with a fixed critical point at 0. When $\lambda \neq 0$, the degree of the map doubles to $2n$ and 0 becomes a pole. Then there is a super-attracting critical point at infinity and $2n$ finite critical points located at the $2n^{th}$ roots of λ. There are, however, only two critical values, $v_\lambda = \pm 2\sqrt{\lambda}$. When n is even, $\pm v_\lambda$ both map onto the same point. When n is odd, the orbits of $\pm v_\lambda$ behave symmetrically with respect to $z \mapsto -z$ under iteration. Thus, we say that there is really only one *free critical orbit*.

The *Julia set* of F_λ, denoted by $J(F_\lambda)$, is defined as the closure of the set of repelling periodic points of F_λ. The complement of the Julia set is called the *Fatou set*. Components of the Fatou set may be *escaping* or *non-escaping*. That is, orbits of points in the Fatou set may eventually escape to infinity or they may be bounded for all time.

There is an open Fatou component containing infinity that maps n-to-1 onto itself. We call this region the *immediate basin of attraction* and denote it B_λ. F_λ is conjugate to z^n on B_λ. Since 0 maps onto infinity, there is an open Fatou component containing 0 which also maps n-to-1 onto B_λ. When this region is disjoint from B_λ, we call it the *trapdoor* and denote it T_λ.

We may partition the parameter plane into subsets according to the location of the associated critical values with respect to the sets B_λ and T_λ. The following theorem, from [7], describes all possible cases for which the critical orbit escapes to infinity.

Theorem 2.1. *(The Escape Trichotomy) Let v_λ be a critical value of F_λ.*

1. *If $v_\lambda \in B_\lambda$, then $J(F_\lambda)$ is a Cantor set of points.*
2. *If $T_\lambda \neq B_\lambda$ and $v_\lambda \in T_\lambda$, then $J(F_\lambda)$ is a Cantor set of concentric simple closed curves surrounding the origin. (This does not occur when $n = 2$.)*

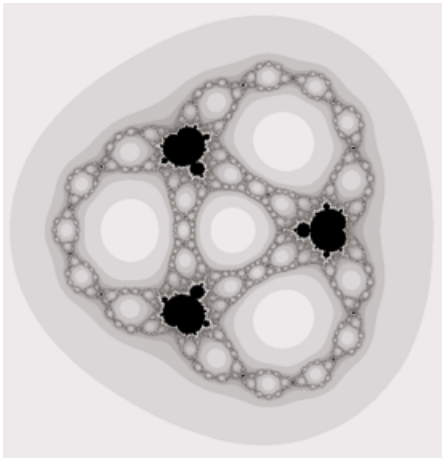

FIGURE 1. The parameter plane for $n = d = 4$.

(3) *Otherwise,* $J(F_\lambda)$ *is a connected set. In particular, if* $T_\lambda \neq B_\lambda$ *and* $F_\lambda^i(v_\lambda) \in T_\lambda$ *for some* $i \geq 1$*, then* $J(F_\lambda)$ *is a Sierpiński curve.*

To illustrate this, we display the parameter plane for $n = d = 4$ in Figure 1. The exterior grey region containing infinity is called the *Cantor set locus* and corresponds to the first part of the theorem. The light grey region at the center containing $\lambda = 0$ is called the *McMullen domain* and corresponds to the second part of the theorem. The additional light grey regions are called *Sierpiński holes* and correspond to the Sierpiński curve Julia sets described in the third part of the theorem.

Also observed in numerically generated diagrams of the parameter plane are small copies of the well-known *Mandelbrot set*. In many cases, standard arguments using polynomial-like maps (such as in [4]) prove the existence of such baby Mandelbrot sets. When λ is chosen from one of these baby Mandelbrot sets, the critical orbit does not escape to infinity and the third part of Theorem 2.1 tells us that the Julia set is connected. Some of these baby Mandelbrot sets are *buried*, that is, they are not *accessible* from the Cantor set locus. Julia sets of maps taken from the main cardioids of one of these buried Mandelbrot sets are known to be Sierpiński curves [5]. In this paper, we investigate the structure of Julia sets corresponding to parameters from the accessible baby Mandelbrot sets.

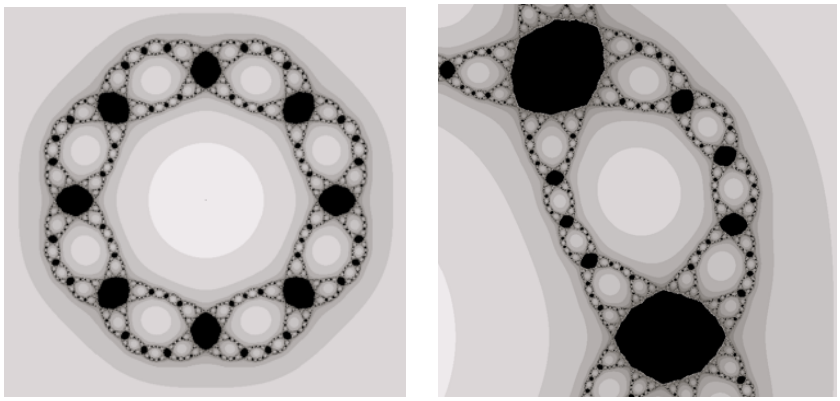

FIGURE 2. A Checkerboard Julia set corresponding to $\lambda = 0.15$ with $n = d = 4$ and a magnification.

3. Checkerboard Julia Sets

We observe that in each parameter plane with $n = d > 2$, there are $n-1$ *principal* accessible Mandelbrot sets [3]. For example, when $n = d = 4$, as in Figure 1, we see three large copies of the Mandelbrot set. Maps taken from the main cardioids of these principal Mandelbrot sets are known to have *Checkerboard* Julia sets [1]. That is, the boundary of each non-escaping Fatou component (colored in black) touches infinitely many boundaries of escaping Fatou components (colored light grey), but it does not touch the boundary of any other non-escaping Fatou component. Similarly, the boundary of any escaping Fatou component touches infinitely many boundaries of non-escaping Fatou components, but it does not touch the boundary of ay other escaping Fatou component, as shown in Figure 2. When $n = d = 2$, we do not have exact copies of the Mandelbrot set, however, there is a large black cardioid-shaped region. Maps taken from this main cardioid also have Checkerboard Julia sets.

For $n = d \geq 2$, any two maps taken from different main cardioids of principal Mandelbrot sets have homeomorphic Julia sets. However, these maps will not necessarily exhibit conjugate dynamics. These facts, as well as a method of determining the exact number of conjugacy classes for such maps, are presented in [1].

If one zooms in on the boundary of the Cantor set locus, one notices additional smaller Mandelbrot sets located symmetrically between the principal Mandelbrot sets. In fact, it appears that there are infinitely many levels of progressively smaller accessible Mandelbrot sets. As in the Checkerboard case, we ask whether maps corresponding to distinct

main cardioids from the same level of accessible Mandelbrot sets will have conjugate dynamics. In the case of $n = d = 2$, we will show that the answer is no, unless the accessible Mandelbrot sets are complex conjugates of one another.

4. External Rays in the Parameter Plane

Consider the case where $n = d = 2$. Just as in the case of the complex quadratic map, there exists a homeomorphism, known as the Böttcher coordinate, which takes straight rays extending out from the closed unit disk to rays in the exterior region of the parameter plane [9]. We associate to each *external ray* an angle between 0 and 1. In particular, the rays having angles of the form $\frac{t}{2^m-1}$ where $m = 2, 3, 4, ...$ and $t = 1, 2, 3, ..., 2^m - 2$, land on hyperbolic components containing parameters corresponding to maps with an orbit of period m [10]. We conjecture that these hyperbolic components are, in fact, main cardioids of baby Mandelbrot sets and the external rays land at the cusps of these cardioids. Maps taken from the same hyperbolic component are known to be quasiconformally conjugate on their Julia sets [8], thus any two parameters in the same main cardioid will have attracting periodic orbits of the same period. The unique λ in each main cardioid for which the critical orbit is super-attracting is called the *center* of the main cardioid. Thus the critical orbit of the map taken from the center of the $\frac{t}{2^m-1}$ Mandelbrot set has period m. We shall restrict our investigation to these points. As an example, the parameter plane and several external rays for $n = d = 2$ are shown in Figure 3.

5. Structure of the Julia Set for $n = d = 2$

The map $F_\lambda(z) = z^2 + \frac{\lambda}{z^2}$ has degree 4 and has four finite critical points. When λ is the center of the main cardioid of an accessible Mandelbrot set, one of the four critical points is periodic. The remaining three critical points are pre-periodic and eventually land on the periodic critical orbit. Thus, all four critical points are located in non-escaping Fatou components. Denote the critical point that lies in the first quadrant by c_1 and proceed counterclockwise about the origin labeling the others c_2, c_3, and c_0. Then let C_i denote the non-escaping Fatou component containing c_i.

Since $F_\lambda^2(z) = F_\lambda^2(iz)$, the Julia set has four-fold symmetry. We conclude that the critical points and corresponding C_i are located symmetrically at quarter-turn intervals about the origin.

By the Escape Trichotomy, we know that the Julia set is connected. Combined with fourfold symmetry, we conclude that B_λ is disjoint from T_λ. Furthermore, since all four critical points lie in non-escaping Fatou

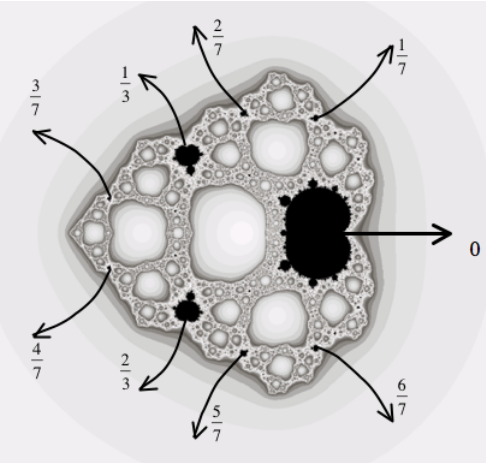

FIGURE 3. External rays in the parameter plane for $n = d = 2$.

components, $\partial B_\lambda \cap \partial T_\lambda$ cannot contain a critical point, so ∂B_λ must be disjoint from ∂T_λ.

When λ is the cusp of the main cardioid of the $\frac{t}{2^m-1}$ Mandelbrot set, F_λ^m has a unique neutral fixed point located at the intersection of the boundary of a non-escaping Fatou component and ∂B_λ. Then, for the map taken from the center of the same main cardioid, the boundary of the C_i containing the periodic critical point c_i must intersect ∂B_λ at a point p_i. Since ∂T_λ maps onto ∂B_λ, the image of p_i under F_λ has a pre-image q_j which must be contained in $\partial T_\lambda \cap \partial C_j$, for some j. Therefore, each ∂C_i has a point, p_i, on ∂B_λ and another point, q_i, on ∂T_λ. For this reason, we call C_i a *connecting* Fatou component (see Figure 4).

F_λ maps B_λ two-to-one onto itself and also maps T_λ two-to-one onto B_λ. Since F_λ has degree 4, this accounts for all possible preimages of points in B_λ. Thus, any eventually escaping points not already located in B_λ must map through T_λ before escaping. (It is for this reason we call T_λ the *trapdoor*.) Since the critical orbit is assumed to be periodic, we know that the critical values cannot lie in any pre-image of T_λ, so these pre-images must map univalently onto T_λ. We conclude that there are four disjoint preimages of T_λ located symmetrically about the origin. We now see that the dynamical plane can be divided into 4 symmetric sectors. Let the sector I_i be defined as the closed region whose boundary is given by the portions of ∂C_i, ∂B_λ, ∂C_{i+1}, and ∂T_λ that are traced out

as one moves counterclockwise from p_i to p_{i+1} to q_{i+1} to q_i and back to p_i in such a way that C_i is included in the interior of I_i.

As proven in [1], F_λ maps each I_i univalently (except at the junction points) over the region that is the complement of the three sets B_λ, $F_\lambda(C_i)$, and $F_\lambda(C_{i+1})$. More specifically, the portion of ∂B_λ in I_i is mapped to half of ∂B_λ, while the portion of ∂T_λ in I_i is mapped to the remaining half of ∂B_λ. By this result it sufficies to focus on only one I_i to understand the entire $J(F_\lambda)$.

Since ∂T_λ intersects the boundaries of four connecting Fatou components, the boundary of each preimage of T_λ must intersect the boundary of a preimage of each of these four connecting Fatou components. We call these Fatou components the *corners* of the preimage of T_λ. We've assumed one C_i with period $m \geq 2$ and all others eventually with period m, so no C_i can be its own preimage. Also $F_\lambda(C_1) = F_\lambda(C_3) = -F_\lambda(C_0) = -F_\lambda(C_2)$. Therefore, if C_1 maps onto C_2, then C_0 maps onto itself, a contradiction. By similar arguments, we see that no C_i can be the preimage of any other because this would imply that at least one is fixed. Therefore, all preimages of the C_i are disjoint from the C_i. Furthermore, the order of the preimages of the C_i, as one travels counterclockwise around the boundary of the preimage of T_λ, must be the same as the order of the C_i themselves. Thus, each sector can be divided into four subsectors. For $k \geq 1$, we denote a k^{th} preimage of T_λ by $T^{-k}_{s_0 \ldots s_{k-1}}$, where $s_j = 0, 1, 2$, or 3 identifies the sector in which the j^{th} image of $T^{-k}_{s_0 \ldots s_{k-1}}$ lands.

We show an example of a Julia set for a map taken from the main cardioid of the $\frac{1}{3}$-Mandelbrot set in Figure 4 and a model of the dynamical plane for the same map in Figure 5.

The following Lemmas are useful in describing the dynamical plane.

Lemma 5.1. *There cannot be more than four connecting Fatou components.*

Proof. Without loss of generality, suppose a fifth connecting component, C_4, exists within the preimage of sector I_1 contained in sector I_0. Note that C_4 does not contain a critical point. As mentioned earlier, $\partial I_0 \cap \partial B_\lambda$ maps to half of ∂B_λ and $\partial I_0 \cap \partial T_\lambda$ maps to the other half of ∂B_λ. Thus the points p_4 and q_4, must map to distinct points in $\partial I_1 \cap \partial B_\lambda$ which lie on opposite sides of the point $F_\lambda(p_1) = F_\lambda(q_1)$. Since ∂B_λ is invariant under F_λ, all forward images of p_4 and q_4 lie in ∂B_λ. All black Fatou components are preimages of the periodic C_i (where $i = 0, 1, 2$, or 3), so there is some minimal k for which $F^k(C_4) = C_i$. C_i intersects ∂B_λ at a single point, p_i. Thus $F^k_\lambda(p_4) = F^k_\lambda(q_4) = p_i$. But C_4 and its first $k-1$ images cannot contain a critical point, so $F^{k-1}_\lambda(C_4)$ must map univalently onto C_i. Therefore, $F^k_\lambda(p_4) \neq F^k_\lambda(q_4)$, a contradiction. □

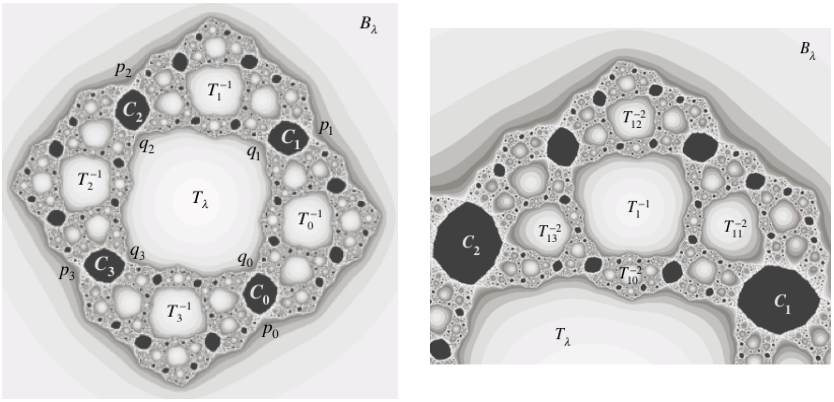

FIGURE 4. The Julia set for λ taken from the $\frac{1}{3}$-Mandelbrot set when $n = d = 2$ and a magnification of sector I_1.

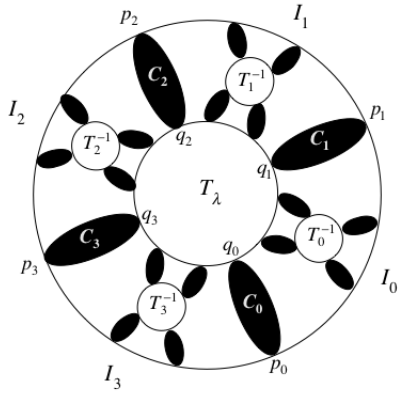

FIGURE 5. A model of the dynamical plane for λ taken from the $\frac{1}{3}$-Mandelbrot set when $n = d = 2$.

Lemma 5.2. *Let λ be the center of the main cardioid of an accessible Mandelbrot set with critical orbit of period $m \geq 2$. Then $T^{-k}_{s_0 s_1 \dots s_{k-1}}$ (with $1 \leq k \leq m$ and $s_j = 0, 1, 2,$ or 3) cannot have all four corners lying on ∂B_λ, nor can $T^{-k}_{s_0 s_1 \dots s_{k-1}}$ have exactly three corners lying on ∂B_λ.*

Proof. By the assumptions $m \geq 2$ and $1 \leq k \leq m$, the corners of $T^{-k}_{s_0 s_1 \dots s_{k-1}}$ must be different from C_{s_0} and C_{s_0+1}. Suppose there exists $T^{-1}_{s_0}$ with all four corners on $\partial B_\lambda \cap \partial I_{s_0}$. Since $\partial B_\lambda \cap \partial I_{s_0}$ maps to half

of ∂B_λ, the images of the four corners of $T_{s_0}^{-1}$, namely the C_i, must all lie on the same half of ∂B_λ. This violates the fourfold symmetry discussed earlier. Now suppose there exists a $T_{s_0 s_1}^{-2}$ having four corners on ∂B_λ, then its image, namely $T_{s_1}^{-1}$, must also have four corners on ∂B_λ, but we have shown that this is not possible. Continue inductively. A similar argument will show that $T_{s_0 s_1 \ldots s_{k-1}}^{-k}$ cannot have exactly three corners on $\partial B_\lambda \cap \partial I_{s_0}$. □

Lemma 5.3. *For λ at the center of the main cardioid of an accessible Mandelbrot set with critical orbit of period greater than or equal to 2, there is exactly one region in each I_i with two corners lying on ∂B_λ and two corners lying on ∂T_λ. Such a region must be T_i^{-1}.*

Proof. Suppose there is a region in I_i with the same structure as T_i^{-1}. Then its image under F_λ will have four corners on ∂B_λ but will be different from T_λ. However, by Lemma 5.2, there are no such regions. □

6. Constructing a Model of the Julia Set for $n = d = 2$

Note that $\overline{F_\lambda(z)} = F_{\bar{\lambda}}(\bar{z})$. Therefore, F_λ is dynamically conjugate to $F_{\bar{\lambda}}$ under complex conjugation and the Julia sets of these maps are homeomorphic. This allows us to restrict our study to the upper-half of the parameter plane and we consider only λ at the centers of the main cardioids of the $\frac{t}{2^m-1}$ Mandelbrot sets with $t = 1, ..., 2^{m-1} - 1$.

If the maps F_λ and F_μ have conjugate dynamics on their Julia sets, we should be able to define a homeomorphism between $J(F_\lambda)$ and $J(F_\mu)$. Furthermore, we expect to find a homeomorphism that takes ∂B_λ to ∂B_μ and ∂T_λ to ∂T_μ. In the argument below, we construct a basic model for the structure of the Julia set and show that no such homeomorphism can exist between two such models, unless the main cardioids with centers λ and μ are complex conjugates of one another.

We remark that the case where all critical points of F_λ are strictly pre-periodic and lie in ∂B_λ was studied in [6]. Such maps are known as *Misiurewicz-Sierpiński* maps or, more succinctly, *MS* maps. The structure of the dynamical plane corresponding to an MS map is similar to the structure for maps with a periodic critical point. For this reason, we use much of the same notation and a similar method for constructing models of the associated Julia sets.

As in our first example, we begin with λ at the center of the main cardioid of the $\frac{1}{3}$-Mandelbrot set. Since $\frac{1}{3}$ has period 2 under the angle-doubling map, we know that one of the critical points of F_λ is periodic with period 2. We identify the connecting Fatou components containing the critical points down to single points which we continue to refer to

as C_i. Likewise, we identify any images or preimages of the C_i down to single points.

It is known that there exists a unique analytic homeomorphism h_λ which takes B_λ to the exterior of the closed unit disk, takes ∞ to ∞, and conjugates F_λ in B_λ to $z \mapsto z^2$ in $\overline{\mathbb{C}} - \overline{\mathbb{D}}$. Define straight rays in $\overline{\mathbb{C}} - \overline{\mathbb{D}}$ by $R_\theta = \left[te^{i\theta} : t > 1\right]$ for $0 \leq \theta < 1$. Then the preimages of these rays under h_λ define *dynamical rays* in B_λ. We then define $H = H(\lambda) = h_\lambda(F_\lambda^2(c_\lambda))$ where c_λ is any of the four critical points. H is an analytic homeomorphism which takes the exterior of the connectedness locus in the parameter plane to $\overline{\mathbb{C}} - \overline{\mathbb{D}}$. Then $H^{-1}(R_\theta)$ defines an *external parameter ray*. Furthermore, since F_λ is hyperbolic on $J(F_\lambda)$, it is known that ∂B_λ is a simple closed curve and we can extend this homeomorphism to the boundary $(h_\lambda : \overline{B_\lambda} \mapsto \overline{\mathbb{C}} - \mathbb{D})$.

Suppose θ is a rational angle between 0 and 1 with period m under the doubling map. Then the parameter ray $H^{-1}(R_\theta)$ lands at a parameter in the boundary of the connectedness locus for which the second iterates of the critical points lie in the immediate basin of a parabolic periodic point on ∂B_λ that is the landing point of the dynamical ray R_θ.

Recall that when n is even, all four critical points map onto the same point after two iterations. In particular, $F_\lambda^2(c_\lambda) = 4\lambda + \frac{1}{4}$. Thus, we have a single free critical orbit whose period under F_λ is the same as the period under the doubling map of the angle of the parameter ray which lands on the Mandelbrot set containing λ.

When $\theta = \frac{t}{2^m - 1}$, there are four possible angles for the dynamical rays that land on connecting Fatou components. The one in the first quadrant is $h_\lambda(C_1)$, given by $\frac{t}{4(2^m-1)}$. The remaining $h_\lambda(C_i)$ (for $i = 2, 3, 0$) are given by the fourfold symmetry.

In our example, λ is taken from the $\frac{1}{3}$-Mandelbrot set. We know that the angles associated to the critical orbit are $\frac{1}{3} \mapsto \frac{2}{3} \mapsto \frac{1}{3}$. Since $\frac{1}{3}$ corresponds to the second iterate of the periodic critical point associated to the cycle, we know that the Fatou component containing the periodic critical point must lie at the landing point of the $\frac{1}{3}$-dynamical ray. This implies that C_2 contains the periodic critical point, so $h(C_2) = \frac{1}{3}$. By symmetry, we compute that $h(C_1) = \frac{1}{12}$, $h\left(C_3\right) = \frac{7}{12}$, and $h\left(C_0\right) = \frac{5}{6}$. Now, the portion of ∂B_λ that lies on the boundary of each I_i is associated to an interval on the unit circle. To avoid ambiguity, we take each C_i to lie in I_i but not in I_{i-1}.

Thus:

$$h_\lambda\left(\partial B_\lambda \cap I_1\right) = \left[\frac{1}{12}, \frac{1}{3}\right)$$

$$h_\lambda\left(\partial B_\lambda \cap I_2\right) = \left[\frac{1}{3}, \frac{7}{12}\right)$$

$$h_\lambda\left(\partial B_\lambda \cap I_3\right) = \left[\frac{7}{12}, \frac{5}{6}\right)$$

$$h_\lambda\left(\partial B_\lambda \cap I_0\right) = \left[\frac{5}{6}, \frac{1}{12}\right).$$

∂B_λ is invariant under F_λ, so all points in the forward orbit of C_2 lie in ∂B_λ. We can now assign an *itinerary* to C_2 according to the behavior of $h_\lambda\left(C_2\right)$ with respect to the aforementioned intervals on the unit circle. Recall that the forward orbit of the dynamical ray landing at C_2 under doubling was given by $\frac{1}{3} \mapsto \frac{2}{3} \mapsto \frac{1}{3}$. This tells us that $C_2 \in \partial I_2$, $F_\lambda\left(C_2\right) \in \partial I_3$, and $F_\lambda^2\left(C_2\right) = C_2 \in \partial I_2$. We define the itinerary of C_2 by $S\left(C_2\right) = \overline{23}$.

We extend the homeomorphism, h_λ, to take ∂T_λ to a simple closed curve contained in $\overline{\mathbb{D}}$, which intersects the unit circle exactly four times at $\frac{1}{12}, \frac{1}{3}, \frac{7}{12}$, and $\frac{5}{6}$. This divides our model into four regions corresponding to the sectors, I_i.

By Lemma 5.3, there is a preimage of T_λ in each I_i, which has two corners on ∂B_λ and two corners on ∂T_λ. Using the angle-doubling map, we can compute precisely the angles associated to the corners of each $h_\lambda\left(T_i^{-1}\right)$. We remark that $h_\lambda\left(F_\lambda\left(C_2\right)\right) = \frac{2}{3}$ corresponds to one of the corners where ∂T_3^{-1} intersects ∂B_λ.

The $h_\lambda\left(T_i^{-1}\right)$ divide each $h_\lambda(I_i)$ into four subsectors which are preimages of the original four sectors. For simplicity and because it causes no confusion, we denote $h_\lambda\left(T_i^{-1}\right)$ by T_i^{-1} and $h_\lambda(I_i)$ by I_i. We denote any of the preimages of I_j contained within I_i by I_{ij}^{-1}. Figure 6 depicts our model as described thus far.

Now each subsector must contain a $T_{s_0 s_1}^{-2}$, which has exactly two corners lying on $\partial T_{s_0}^{-1}$. We refer to the other two corners of $T_{s_0 s_1}^{-2}$ as the *free corners*. Since $F_\lambda^2\left(C_2\right) = C_2$, one of the free corners of T_{23}^{-2} must be C_2. The other free corner of T_{23}^{-2} must lie in $\partial I_{23}^{-1} \cap \left(\partial B_\lambda \cup \partial T_\lambda\right)$.

To determine the specific location of this corner, we recall that F_λ preserves orientation of points along any preimage of ∂B_λ. This allows us to compare the order of the free corners of T_{23}^{-2} along $\partial I_{23}^{-1} \cap \left(\partial B_\lambda \cup \partial T_\lambda\right)$ to the order of their forward images along ∂I_3. The point where ∂T_2^{-1} intersects $\partial I_{23}^{-1} \cap \partial B_\lambda$ maps to $C_0 = \frac{5}{6}$, the point where ∂T_2^{-1} intersects $\partial I_{23}^{-1} \cap \partial T_\lambda$ maps to $C_3 = \frac{7}{12}$, and C_2 maps to $\frac{2}{3}$. Since the second free corner of T_3^{-1} lies between $\frac{2}{3}$ and $\frac{5}{6}$, we conclude that the second free corner of T_{23}^{-2} lies between the point where ∂T_2^{-1} intersects $\partial I_{23}^{-1} \cap \partial B_\lambda$ and the point C_2. We now have a topological invariant, which we call a

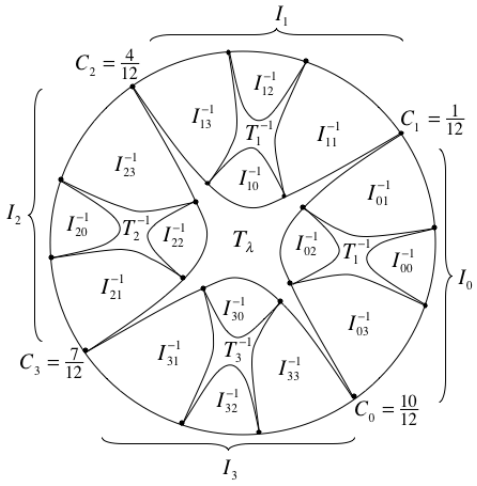

FIGURE 6. A model of the dynamical plane for λ taken from the $\frac{1}{3}$-Mandelbrot set when $n = d = 2$.

chain of preimages of T_λ. When the critical point c_i has period m and itinerary $S(c_i) = is_1...s_{m-1}$, we consider a chain of preimages of T_λ to be the collection $\{T_\lambda, T_i^{-1}, T_{is_1}^{-2}, T_{is_1s_2}^{-3}, ..., T_{is_1s_2...s_{m-1}}^{-m}\}$.

The structure of T_{23}^{-2} and the chain of preimages of T_λ are illustrated in Figure 7. We observe that the structure of this model corresponds to the structure exhibited by the Julia set in Figure 4.

Consider the map F_μ associated to the parameter μ taken from the main cardioid of a different accessible Mandelbrot set. If there exists a homeomorphism between $J(F_\lambda)$ and $J(F_\mu)$ which sends ∂B_λ to ∂B_μ and ∂T_λ to ∂T_μ, then the homeomorphism must preserve the structure of this chain of preimages of T_λ. It is clear that for any map with critical orbit of period m, the chain of preimages contains T_λ and m of its preimages. Therefore, since $\frac{1}{3}$ is the only period 2 angle in the upper halfplane, we immediately conclude that there is no such homeomorphism between the Julia set associated to a map from the $\frac{1}{3}$-Mandelbrot set and the Julia set of a map taken from any other main cardioid in the upper halfplane. We recall, however, that maps taken from the $\frac{1}{3}$-Mandelbrot set and maps taken from the $\frac{2}{3}$-Mandelbrot set do have conjugate dynamics on their Julia sets.

Next, we examine the three accessible Mandelbrot sets in the upper halfplane that have critical orbits of period 3. These are the $\frac{1}{7}$, $\frac{2}{7}$, and $\frac{3}{7}$-Mandelbrot sets. We will see that the structure of the chain of preimages

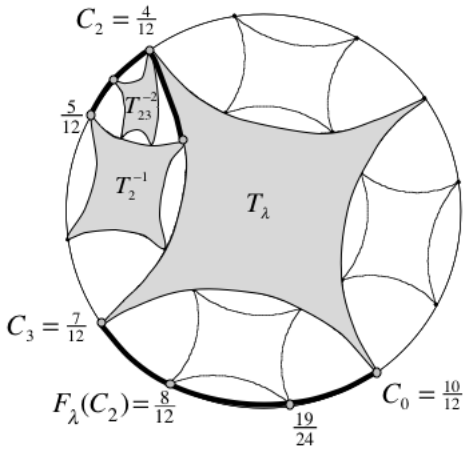

FIGURE 7. The chain of preimages of T_λ for λ taken from the $\frac{1}{3}$-Mandelbrot set when $n = d = 2$. The highlighted portion of ∂I_{23}^{-1} maps to the highlighted portion of ∂I_3 under F_λ.

of T_λ is uniquely determined by the itinerary of the the periodic critical point which is, in turn, unique to the chosen Mandelbrot set.

Take, for example, λ at the center of the main cardioid of the $\frac{2}{7}$-Mandelbrot set. We know the angles associated to the critical orbit are $\frac{2}{7} \mapsto \frac{4}{7} \mapsto \frac{1}{7} \mapsto \frac{2}{7}$. Since $\frac{2}{7}$ corresponds to the second iterate of the periodic critical point associated to the cycle, we know that the Fatou component containing the periodic critical point must lie at the landing point of the $\frac{4}{7}$-dynamical ray. This implies that C_3 contains the periodic critical point, so $h_\lambda(C_3) = \frac{4}{7}$. By symmetry, we compute that $h_\lambda(C_1) = \frac{1}{14}$, $h_\lambda(C_2) = \frac{9}{28}$, and $h_\lambda(C_0) = \frac{23}{28}$. This again divides the unit circle into four intervals.

$$h_\lambda\left(\partial B_\lambda \cap I_1\right) = \left[\frac{1}{14}, \frac{9}{28}\right)$$

$$h_\lambda\left(\partial B_\lambda \cap I_2\right) = \left[\frac{9}{28}, \frac{4}{7}\right)$$

$$h_\lambda\left(\partial B_\lambda \cap I_3\right) = \left[\frac{4}{7}, \frac{23}{28}\right)$$

$$h_\lambda\left(\partial B_\lambda \cap I_0\right) = \left[\frac{23}{28}, \frac{1}{14}\right).$$

We now assign an itinerary to C_3 according to the behavior of $h_\lambda(C_3)$ with respect to these four intervals. Recall that the forward orbit of the periodic dynamical ray landing at C_3 under doubling is given by $\frac{2}{7} \mapsto \frac{4}{7} \mapsto \frac{1}{7} \mapsto \frac{2}{7}$. This tells us that $C_3 \in \partial I_3$, $F_\lambda(C_3) \in \partial I_1$, $F_\lambda^2(C_3) \in \partial I_1$, and $F_\lambda^3(C_3) = C_3 \in \partial I_3$. We define the itinerary of C_3 as $S(C_3) = \overline{311}$. This itinerary will be useful in constructing the chain of preimages of T_λ in the model of $J(F_\lambda)$.

The chain will include T_λ, T_3^{-1}, T_{31}^{-2}, and T_{311}^{-3}. To give a full description of the structure of the chain, we determine the location of the corners of each element of the chain. We already know that the four corners of T_λ lie on ∂B_λ and that T_3^{-1} has two corners on ∂B_λ and two corners on ∂T_λ.

T_3^{-1} divides I_3 into four subsectors. T_{31}^{-2} is contained in I_{31}^{-1} and the four corners of T_{31}^{-2} lie on ∂I_{31}^{-1}. Exactly two corners of T_{31}^{-2} lie in ∂T_3^{-1}, so the two free corners of T_{31}^{-2} must lie in $\partial I_{31}^{-1} \cap (\partial B_\lambda \cup \partial T_\lambda)$. As in our previous example, the order of points along this curve is preserved under F_λ.

The point $\partial I_{31}^{-1} \cap \partial T_\lambda \cap \partial T_3^{-1}$ maps to C_1. The free corners of T_{31}^{-2} map to the free corners of T_1^{-1} in ∂B_λ. C_3 maps to a point on the boundary of I_{11}^{-1}. $F_\lambda(C_3)$ lies between C_1 and the free corners of T_1^{-1} along the curve $\partial B_\lambda \cap \partial I_1$. Therefore, C_3 must lie between the point $\partial I_{31}^{-1} \cap \partial T_\lambda \cap \partial T_3^{-1}$ and the free corners of T_{31}^{-2} along the curve $\partial I_{31}^{-1} \cap (\partial B_\lambda \cup \partial T_\lambda)$, see Figure 8.

T_{311}^{-3} has two corners on ∂T_{31}^{-2} and two free corners which map onto the two free corners of T_{11}^{-2}. Since C_3 has period 3, one free corner of T_{311}^{-3} must be C_3 (in other words, C_3 is the preimage of one of the free corners of T_{11}^{-2}). It remains to find the location of the second free corner of T_{311}^{-3}, which must lie in $\partial I_{311}^{-2} \cap (\partial B_\lambda \cup \partial T_\lambda)$.

By symmetry, T_{11}^{-2} has the same structure as T_{31}^{-2}. This allows us to conclude that T_{11}^{-2} also has its two free corners on ∂B_λ. The free corners of T_{11}^{-2} then map onto the free corners of T_1^{-1} and the free corners of T_1^{-1} map onto C_2 and C_3.

In particular, we note that we must move clockwise along $\partial B_\lambda \cap \partial I_1$ to get from $F^{-1}(C_2)$ to $F^{-1}(C_3)$ and clockwise along $\partial B_\lambda \cap \partial I_{11}^{-1}$ to get from $F^{-2}(C_2)$ to $F^{-2}(C_3)$. Similarly, we move clockwise along $\partial I_{311}^{-2} \cap (\partial B_\lambda \cup \partial T_\lambda)$ to get from $F^{-3}(C_3) = C_3$ to the second free corner of T_{311}^{-3},see Figure 8. The complete chain of preimages of T_λ for this example is illustrated in Figure 9.

We then ask whether the chains of preimages of T_λ for maps taken from other accessible Mandelbrot sets with period 3 critical orbits will necessarily have the same structure. A quick glance at the numerically generated

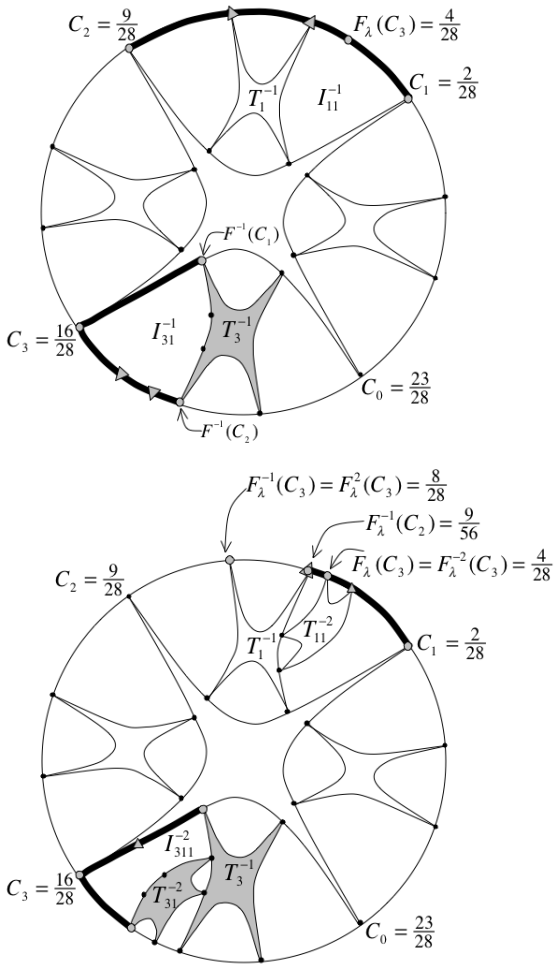

FIGURE 8. Locating the corners of T_{31}^{-2} and T_{311}^{-3} for λ taken from the $\frac{2}{7}$-Mandelbrot set when $n = d = 2$. In the top figure, the highlighted portion of ∂I_{31}^{-1} maps onto the highlighted portion of ∂I_1. In the bottom figure, the highlighted portion of ∂I_{311}^{-2} maps onto the highlighted portion of ∂I_{11}^{-1}.

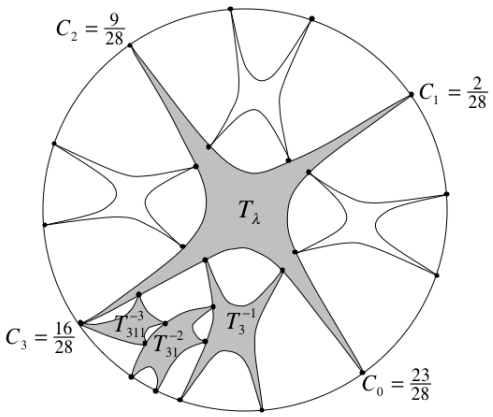

FIGURE 9. The final chain of preimages of T_λ for λ taken from the $\frac{2}{7}$-Mandelbrot set when $n = d = 2$.

dynamical planes for maps taken from the $\frac{1}{7}$, $\frac{2}{7}$, and $\frac{3}{7}$-Mandelbrot sets (see Figure 10) might suggest that a homeomorphism exists between their Julia sets. However, using the same method as before, we construct the chains of preimages of T_λ for the $\frac{1}{7}$ and $\frac{3}{7}$-Mandelbrot sets. It is clear from the structures of these chains (also shown in Figure 10) that no two of these maps can have homeomorphic Julia sets. We conclude that maps taken from the main cardiois of distinct accessible period-3 Mandelbrot sets cannot have conjugate dynamics on their Julia sets, unless these cardioids are complex conjugates of one another.

Next, we consider maps with critical orbits of period greater than 3. Our method for constructing chains will continue to prove useful. However, as the period increases, we see that constructing the chains becomes more complicated. In our previous examples, the free corners of each T^{-k} have fallen either on ∂B_λ or ∂T_λ, but this is not always the case. Sometimes, the free corners of a T^{-k} will fall on the boundary of some T^{-j} with $j < k$.

Take for example, λ at the center of the main cardioid of the $\frac{6}{15}$-Mandelbrot set. We know the angles associated to the critical orbit are $\frac{3}{5} \mapsto \frac{1}{5} \mapsto \frac{2}{5} \mapsto \frac{4}{5} \mapsto \frac{3}{5}$. Since $\frac{3}{5}$ corresponds to the second iterate of the periodic critical point associated to the cycle, we know that the Fatou component containing the periodic critical point must lie at the landing point of the $\frac{2}{5}$ dynamical ray. This implies that C_3 contains the periodic critical point, so $h_\lambda(C_3) = \frac{2}{5}$. By symmetry, we compute that $h_\lambda(C_1) = \frac{1}{10}$, $h_\lambda(C_2) = \frac{7}{20}$, and $h_\lambda(C_0) = \frac{17}{20}$. This again divides the unit

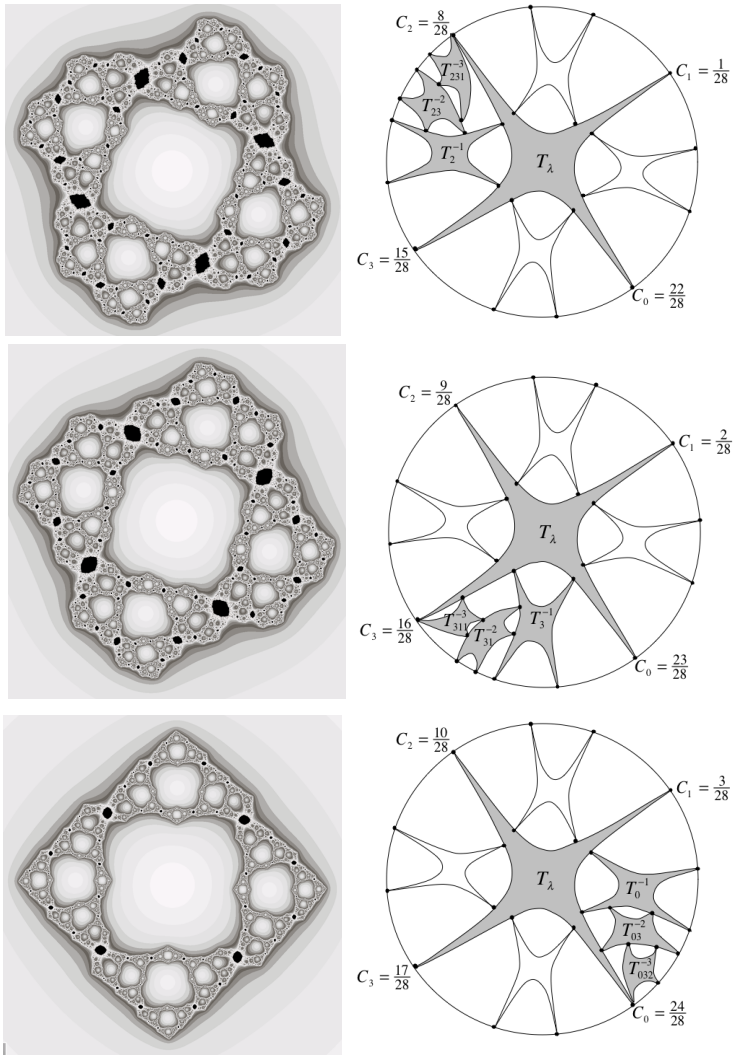

FIGURE 10. The dynamical planes and the corresponding Julia set models for maps taken from the $\frac{1}{7}$, $\frac{2}{7}$, and $\frac{3}{7}$-Mandelbrot sets, respectively, when $n = d = 2$. At first glance, these Julia sets may appear homeomorphic. Comparison of their models clearly shows that this is not the case.

circle into four intervals.

$$h_\lambda\left(\partial B_\lambda \cap I_1\right) = \left[\frac{1}{10}, \frac{7}{20}\right)$$

$$h_\lambda\left(\partial B_\lambda \cap I_2\right) = \left[\frac{7}{20}, \frac{3}{5}\right)$$

$$h_\lambda\left(\partial B_\lambda \cap I_3\right) = \left[\frac{3}{5}, \frac{17}{20}\right)$$

$$h_\lambda\left(\partial B_\lambda \cap I_0\right) = \left[\frac{17}{20}, \frac{1}{10}\right).$$

Since $\frac{3}{5}$ has period 4 under doubling, we conclude that C_3 contains the periodic critical point and its itinerary is given by $S(C_3) = \overline{3123}$.

C_3 must lie within I_{31}^{-1}, which implies that C_3 falls between the free corners of T_{31}^{-2}. Thus one free corner of T_{31}^{-2} lies on ∂B_λ and the other lies on ∂T_λ. C_3 must also lie within I_{312}^{-2}, which implies that both free corners of T_{312}^{-3} lie on ∂B_λ between C_3 and the free corner of T_{31}^{-2} that lies on ∂B_λ. So far, our method has progressed just as in our previous examples. Next, we know that C_3 is one corner of T_{3123}^{-4} and we need only find the location of a single free corner of T_{3123}^{-4}. This free corner lies on ∂I_{3123}^{-3}. Recall that each preimage of T_λ has exactly two corners on a previous preimage of T_λ, this implies that the free corner of T_{3123}^{-4} cannot lie in the section of ∂I_{3123}^{-3} that intersects ∂T_{312}^{-3}. Thus, the free corner lies either on $\partial B_\lambda \cap \partial I_{3123}^{-3}$ or $(\partial T_\lambda \cup \partial T_{31}^{-2}) \cap \partial I_{3123}^{-3}$. $F_\lambda^3(C_3)$ is the corner of T_3^{-1} in ∂T_λ closest to C_0. This implies that the free corner of T_{3123}^{-4} lies in $(\partial T_\lambda \cup \partial T_{31}^{-2}) \cap \partial I_{3123}^{-3}$. To complete the model, we just determine whether this free corner lies on ∂T_λ or ∂T_{31}^{-2}. The point $\partial T_\lambda \cap \partial T_{31}^{-2}$ divides these two curve segments. By comparing the forward images of this point to the forward images of the free corner of T_{3123}^{-4} and using the fourfold symmetry of the Julia set, we can determine the that the free corner lies on ∂T_{31}^{-2}. The model of this Julia set can be seen in Figure 11.

7. Conclusion

There is a rational parameter ray corresponding to each accessible Mandelbrot set. This rational angle corresponds to a unique itinerary for the periodic critical point of a map taken from center of the main cardioid of this Mandelbrot set. The itinerary determines the model for the Julia set of the map. Thus, each ray defines a unique model. Likewise, given a model, one can determine the unique corresponding itinerary. This allows us to conclude the following:

For $n = d = 2$, given parameters λ and μ from the main cardioids of

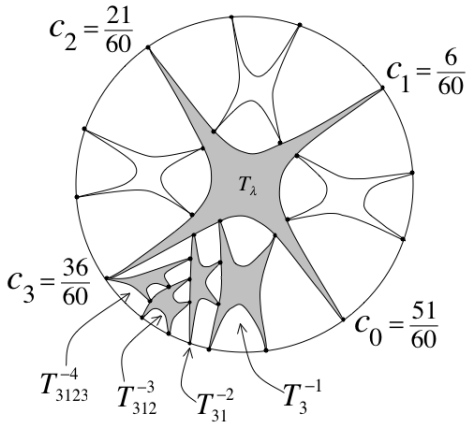

FIGURE 11. A model of the dynamical plane for λ taken from the $\frac{6}{15}$ Mandelbrot set when $n = d = 2$.

different accessible Mandelbrot sets, there exists a homeomorphism taking ∂B_λ *to* ∂B_μ *and* ∂T_λ *to* ∂T_μ *if and only if* $\mu = \overline{\lambda}$.

In ongoing work, we consider cases of $n = d > 2$ and we conjecture that the same result will hold. We have found that, when n is odd, the construction of the models can be more challenging because there are always two periodic critical points. Sometimes these points lie on the same orbit of period $2n$ and other times each periodic critical point has a unique orbit of period n. Construction of these models is made easier by considering a map which is semi-conjugate to F_λ but has a single critical point.

We reiterate the distinction between our results those for the principal Mandelbrot sets. Each map taken from the main cardioid of a principal Mandelbrot set is known to have a Checkerboard Julia set. The Julia sets corresponding to maps taken from the main cardioids of distinct principal Mandelbrot sets are known to be homeomorphic and, in some cases, these maps exhibit conjugate dynamics on their Julia sets. In contrast, when we consider maps taken from main cardioids of distinct accessible Mandelbrot sets of period $m \geq 2$, we have seen that the corresponding Julia sets cannot be homeomorphic and thus, such maps can never exhibit conjugate dynamics on their Julia sets.

References

[1] P. Blanchard, F. Cilingir, D. Cuzzocreo, R. L. Devaney, D. Look, E. D. Russell, *Checkerboard Julia sets for rational maps*, Internat. J. Bifur. Chaos Appl. Sci. Engrg. **23** (2013)

[2] R. L. Devaney, *A myriad of Sierpiński curve Julia sets*, Difference Equations, Special Functions, and Orthogonal Polynomials. World Scientific, (2007), 131–148.

[3] R. L. Devaney, *Baby Mandelbrot sets adorned with halos in families of rational maps*, Complex Dynamics: Twenty-Five Years After the Appearance of the Mandelbrot Set, American Mathematical Society. Contemporary Math, **396** (2006), 37–50.

[4] R. L. Devaney, *A Cantor-Mandelbrot-Sierpiński tree in the parameter plane for rational maps*, Transactions of the AMS (to appear)

[5] R. L. Devaney, D. Look, *Buried Sierpiński curve Julia sets*, Discrete Cont. Dyn. Syst. Am. Inst. Math. Sci. **13** (2005), no. 4, 1035–1046.

[6] R. L. Devaney, M. Moreno Rocha, S. Siegmund, *Rational maps with generalized Sierpiński gasket Julia sets*, Topology Appl. **154** (2007), no. 1, 11–27. doi: 10.1016/j.topol.2006.03.024

[7] R. L. Devaney, D. Look, D. Uminsky, *The Escape Trichotomy for singularly perturbed rational maps*, Indiana Univ. Math. J. **54** (2005), 1621–1634 .

[8] R. Mañé, P. Sad, D. Sullivan, *On the dynamics of rational maps*, Annales Scientifiques de l'École Normale Supérieure, Quatrième Série, **16** (1983), 193–217.

[9] J. Milnor, *Dynamics in One Complex Variable*. 3rd edn. (Annals of Mathematics Studies, Princeton University Press, 2006)

[10] C. Petersen, G. Ryd, *Convergence of rational rays in parameter spaces*, The Mandelbrot set: Theme and Variations, London Mathematical Society, Lecture Note Series 274, Cambridge University Press, (2000), 161–172 .

Department of Mathematics and Statistics; Boston University; Boston, Massachusetts 02215

E-mail address: lizfitz@bu.edu

Department of Mathematics and Statistics; Boston University; Boston, Massachusetts 02215

E-mail address: stefanos@bu.edu